

# The Age of Ellipticals and the Color-Magnitude Relation

James Schombert

*Department of Physics, University of Oregon, Eugene, OR 97403; js@abyss.uoregon.edu*

Karl Rakos

*Institute for Astronomy, University of Vienna, A-1180, Wien, Austria; karl.rakos@chello.at*

## ABSTRACT

Using new narrowband color observations of early-type galaxies in clusters, we reconstruct the color-magnitude relation (CMR) with a higher degree of accuracy than previous work. We then use the spectroscopically determined ages and metallicities from three samples (Trager *et al.* 2008, Thomas *et al.* 2005, Gallazzi *et al.* 2006), combined with multi-metallicity SED models, to compare predicted colors for galaxies with young ages (less than 8 Gyr) with the known CMR. We find that the CMR cannot be reproduced by the spectroscopically determined ages and metallicities in any of the samples despite the high internal accuracies to the spectroscopic indices. In contrast, using only the  $\langle \text{Fe} \rangle$  index to determine  $[\text{Fe}/\text{H}]$ , and assuming a mean age of 12 Gyr for a galaxy's stellar population, we derive colors that exactly match not only the color zero-point of the CMR but also its slope. We consider the source of young age estimates, the  $H\beta$  index, and examine the conflict between red continuum colors and large  $H\beta$  values in galaxy spectra. We conclude that our current understanding of stellar populations is insufficient to correctly interpret  $H\beta$  values and that the sum of our galaxy observations supports an old and monolithic scenario of galaxy formation. *This result has a devastating impact on every study that has used the  $H\beta$  index to calculate galaxy age, as the use of the  $H\beta$  versus  $\text{MgFe}$  diagram will result in incorrectly deduced young ages.*

*Subject headings:* galaxies: evolution – galaxies: elliptical

## 1. INTRODUCTION

The fundamental concepts in the fields of cosmology and galaxy formation hinge on the one defining characteristic of galaxies, their age. However, a galaxy's age is a difficult parameter to define observationally. For example, in the current cold dark matter paradigm ( $\Lambda$ CDM, Bahcall *et al.* 1999), a galaxy's age is the point in time when the non-baryonic matter becomes gravitational bound. These dark matter halos, then, induce the infall of baryonic material, that forms the luminous galaxies that we observe. Typically, a collection of raw dark and baryonic matter is

impossible to date as they contain no signatures of age (i.e. an observable clock). Only if, and when, the baryonic matter collapses and initiates star formation do we have any measure of the amount of time since the formation epoch.

A complication arises if the time of initial star formation does not immediately follow the epoch of gravitational collapse. If star formation is delayed, the age of the stellar population will not coincide with the formation age. Fortunately, studies of globular clusters have revealed that there do exist stars in our own Galaxy with ages that are nearly equal to the age of the Universe (Marin-Franch *et al.* 2008; Salaris & Weiss 2002). Therefore, even if star formation is ongoing through a galaxy’s life, it may be possible to isolate the oldest stars and use their ages as a lower limit to the age of the entire galaxy system and, by inference, the epoch of galaxy formation.

In addition to a possible mismatch between the epoch of formation and the epoch of initial star formation, there is also the possibility that the stars in a galaxy do not form instantaneously as one unit. For example, in our own Galaxy there is a range of stellar ages (Twarog 1980), although the halo population is uniformly old (De Angeli *et al.* 2005). This problem can be minimized by focusing our studies on galaxies where there is no evidence of current or recent star formation. Early-type galaxies satisfy this condition with their lack of molecular gas and spectra profiles that are dominated by evolved stars suggesting a majority are older than a few Gyr (see Trager *et al.* 2005 for a dissenting view).

The age of a galaxy’s stellar population has become an increasingly important parameter in the last decade with the introduction of hierarchical models of galaxy formation. Under the original scenarios of galaxy formation (referred to as the monolithic model, Larson 1974; Kodama & Arimoto 1997), a galaxy forms quickly, with an intense epoch of star formation at high redshifts followed by a short phase of galactic winds. The rapid initial star formation produces a stellar population that is nearly singular in age and uniform in its chemical composition. The epoch of galactic winds is controlled by a galaxy’s mass (i.e. depth of its gravitational potential) and, thereby, its total metallicity. Under hierarchical models, the formation epochs are extended to lower redshifts, assumingly with later epochs of star formation and thereby younger stellar ages (White & Frenk 1991).

The history of determining the age of a galaxy’s stellar population is long and rich in observational techniques (see Thomas *et al.* 2005 for a review). Early studies focused on the direct comparison between integrated galaxy colors and colors of galactic clusters (Sandage & Vishvanathan 1977; Burstein *et al.* 1987). These early results supported a view where early-type galaxy stellar populations were similar to globular clusters in their evolutionary state, but with higher metallicities (Burstein *et al.* 1984). Improved technology led to the matching of colors with various spectral indices (Gonzalez 1993; Trager *et al.* 2000). And improved spectroenergy distribution (SED) models led to the use of spectral indices alone to calculate the age and metallicity of underlying stellar populations (Kuntschner 2000; Trager *et al.* 2000).

The method of determining age and metallicity of a galaxy matured with the introduction of

the Lick system that, primarily, depends on Fe (notably Fe5270 and Fe5335), Mg *b* and H $\beta$  lines to deduce mean age and metallicity (Trager *et al.* 2000). A surprising result from the spectroscopic surveys (e.g., Gallazzi *et al.* 2006) is that a significant fraction of early-type galaxies have mean ages younger than expected from monolithic scenarios (see Schiavon 2007 for a review). This result would support hierarchical models of galaxy formation (Kauffmann, White & Guiderdoni 1993; Cowie *et al.* 1996).

A range of ages for early-type galaxies is not necessarily a problem for their optical and near-IR colors as a stellar population’s color evolution is expected to proceed at a rapid pace for the first 1 to 2 Gyr after initial star formation, but color changes over the next 10 Gyr are small (Bower *et al.* 1992). However, a significant number of early-type galaxies with ages less than 8 Gyr would challenge our understanding of the thinness of the Fundamental Plane (MacArthur *et al.* 2008; Cappellari *et al.* 2006, where galaxies greater than  $10^{11}M_{\odot}$  have formation redshifts of greater than 2); the detection of evolved galaxies at high redshifts (Mei *et al.* 2009, Andreon *et al.* 2008, where both studies find passive evolution with redshifts of formation beyond 3); and the passive evolution of galaxies at intermediate redshifts (Kelson *et al.* 2001, Rakos & Schombert 1995, where both studies find colors and spectral indices agree with passive evolution models to redshifts of 0.8).

The goal of this paper is to examine the impact of young stellar population age by comparison of expected colors for galaxies with spectroscopically determined ages and metallicity against the color-magnitude relation (CMR). Due to the known lack of uniqueness in age and metallicity for broadband color systems (i.e. Johnson *UBV* or SDSS *gri*, Worthey 1994), we compare the SED model generated colors to a special narrowband color system that focuses on spectral regions near the 4000Å break. To achieve this goal, we have divided our analysis into three parts. First, we examine the behavior of the CMR in our color system and compare its slope and zeropoint to other CMR’s. Second, we outline the selected SED models and their input parameters. Lastly, we construct CMR’s from actual spectroscopic samples and compare their colors with our observations. Anticipating that the derived colors, across all wavelengths, will be too blue to reproduce the observed CMR, we will also examine the color-H $\beta$  phase space in order to isolate the magnitude of the discrepancies.

## 2. Color-Magnitude Relation

Perhaps one of the oldest galaxy correlations is the one between galaxy absolute luminosity and its global color (i.e., the color-magnitude relation, Baum 1959; Faber 1973; Visvanathan & Sandage 1977). While first discovered in near-UV and blue wavelengths (Caldwell 1983), subsequent studies have demonstrated its existence from the far-UV (Kaviraj *et al.* 2007) to the near-IR (Chang *et al.* 2006). All these studies can be summarized such that 1) the correlation is one of redder galaxy colors with increasing galaxy luminosity, 2) the correlation exists over a range of galaxy environments, but strongest in the densest regions (Cooper *et al.* 2008), 3) the scatter in the

correlation for early-type galaxies, while small, is greater than observational errors (although most of the scatter is associated with star-forming galaxies, Andreon 2003), 4) scatter for early-type galaxies increases as the environment density decreases and 5) there exist distinct red and blue components to the CMR, with the red component being composed of early-type galaxies (Baldry *et al.* 2006).

Several direct corollaries are derived from the CMR with additional knowledge concerning a galaxy’s luminosity and color. The first is that galaxy luminosity is directly tied to the stellar mass of a galaxy (Bernardi *et al.* 2003). For early-type galaxies, this is the primary component of their total baryonic mass. The scaling factor from luminosity to stellar mass is the  $M/L$  ratio, that varies in a linear fashion from 2.5 to 5 for luminosities greater than  $-17$  (Bernardi *et al.* 2003; Pahre, Djorgovski & de Carvalho 1998; Kelson *et al.* 2000) and is not a major source of error in later derived relationships between mass and color. The conversion of luminosity to stellar mass is also confirmed by the behavior of the color- $\sigma$  relation, the CMR’s counterpart using a galaxy’s velocity dispersion instead of luminosity (Graves, Faber & Schiavon 2008).

While a galaxy magnitude is directly related to stellar mass, the color of a galaxy is a much more complicated observable to interpret. For early-type galaxies, a majority of a galaxy’s spectrum is dominated by light from the photospheres of the underlying stellar population; however, different spectral regions are sensitive to different types of stars. For example, near-UV colors reflect the contribution of hot stars (Kaviraj 2007). Typically, these are massive, young stars, but the contribution from metal-poor HB stars or blue stragglers can not be ignored (Atlee, Assef & Kochanek 2008; Lisker & Han 2008 ; Yi 2008). The optical and near-IR portions of the spectrum are strongly influenced by stars on the RGB and, to a lesser extent, by turnoff stars (Pickles 1985; Rose 1985). Where colors are dominated by the RGB, then changes in those colors reflect changes in the mean effective temperature of the RGB stars. Since changes in age of RGB stars has very little effect on their temperatures (Charlot & Bruzual 1991), then changes in the color of the RGB is due, primarily, to changes in mean metallicity (Matteucci 2006).

The dominance of the RGB to early-type galaxy colors was the primary reason that the CMR, for this class of galaxies, was presumed to be a metallicity effect (Faber 1973; Larson 1974). Increases in the metallicity of a stellar population lead to a decrease in RGB effective temperature (through increased line blanketing) and, therefore, a redder integrated color. In later studies, Worthey, Trager & Faber (1995) showed that an age-luminosity correlation could also fit the CMR data due to an age-metallicity degeneracy for broadband colors. However, studies of high redshift clusters (Kodama & Arimoto 1997) discouraged an age interpretation since the evolution of the CMR with redshift is less than predicted by a passive evolution model (where it was assumed that a majority of the stellar mass in a galaxy formed at high redshifts, i.e. old, in a rapid burst, and later changed solely by stellar evolutionary effects).

Regardless of whether the CMR is due to age and/or metallicity effects, there is no doubt that the CMR (and its cousin, the color- $\sigma$  relation) relates the luminous and dynamical masses of a

### 1,104 rich cluster galaxies

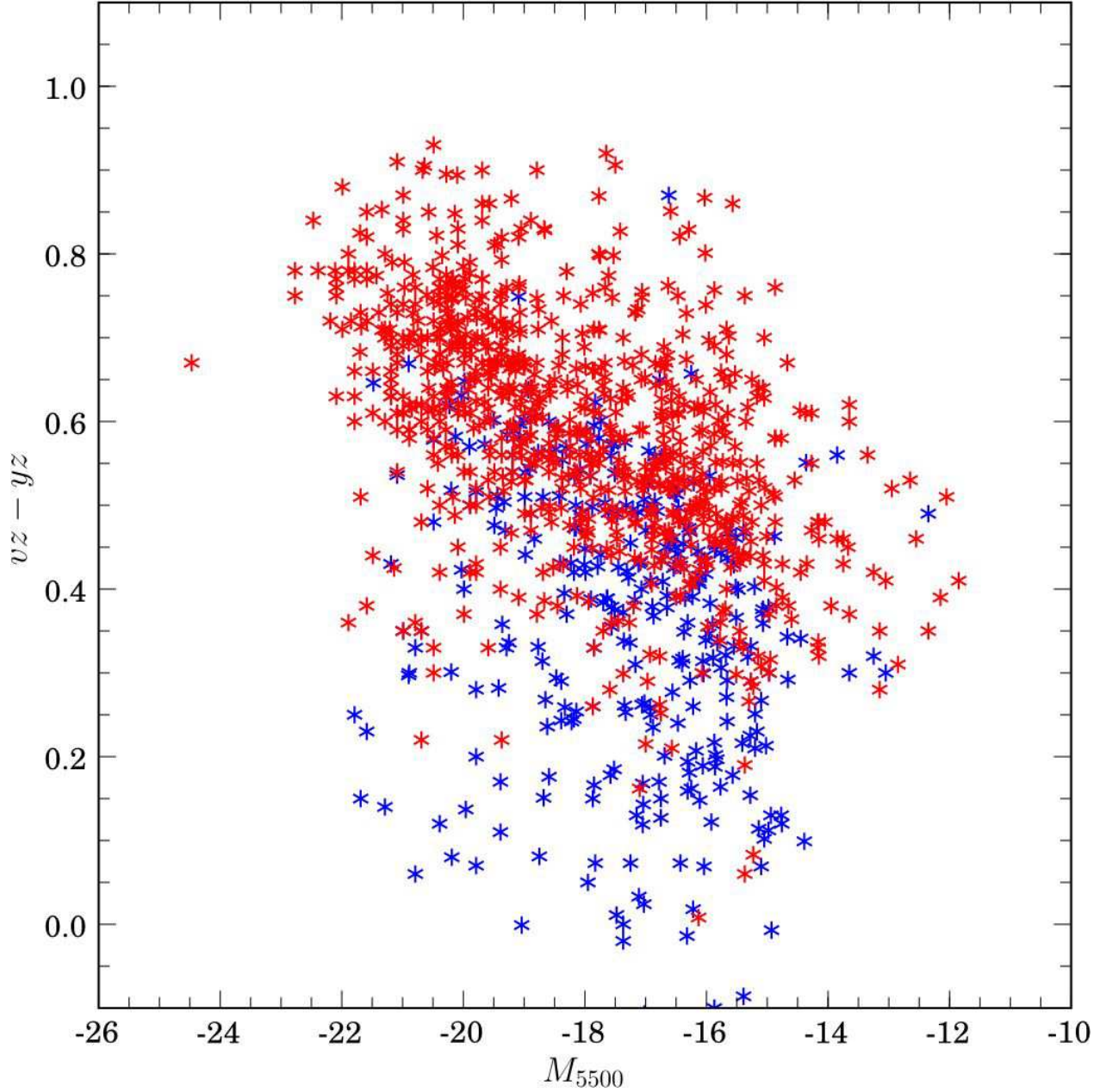


Fig. 1.— The color-magnitude relation for 1,104 galaxies in our cluster sample through our ‘metallicity color’,  $vz - yz$  ( $4100\text{\AA} - 5500\text{\AA}$ ). The red and blue cluster populations are defined by division in our ‘continuum color’,  $bz - yz$ . The red population ends up being 95% early-type galaxies by morphology and produces the strongest correlation between color and luminosity of any filter combination (broadband or narrowband).

galaxy with the properties of its underlying stellar populations. And even evolution models that attribute some of the CMR to the influence of age (younger galaxies have lower luminosities), a majority of the color change must be due to changes in metallicity (Thomas *et al.* 2005). Higher metallicities with higher luminosity (i.e., higher stellar or dynamic mass), as implied by the CMR, can be produced by various galaxy formation scenarios. Each of these scenarios must result in the early cessation of star formation and/or more inefficient chemical evolution for lower mass galaxies. The typical scenario (i.e. a classical wind model) requires rapid enrichment by initial star formation with the chemical enrichment process halted by the removal of a galaxy’s ISM through SN driven galactic winds (Larson 1974, Matteucci & Tornambe 1987).

The difficulty in distinguishing age and metallicity effects on the CMR is particularly salient for broadband filters, such as the Johnson *UBV* system, as demonstrated by Worthey (1994). In fact, under a rapid, single initial burst scenario (the usually assumed scenario of galaxy formation for early-type galaxies), broadband colors achieve stable values after only 3 to 4 Gyr (Bower *et al.* 1992). This limits the ability of CMR to test age versus metallicity effects and the traditional method of overcoming this limitation is to extend the wavelength coverage, for example, using optical to near-IR colors. However, additional complications arise with near-IR colors and the age-metallicity degeneracy concerning RGB and AGB ancestors of high mass stars (Cordier *et al.* 2007).

An alternative approach, with respect to broadband colors, was pioneered by Rakos & Fialia (1983) with the use of optical narrowband filters ( $\Delta\lambda = 200\text{\AA}$ ) based on the Strömrgren system. In this filter system, two of the filters (*bz* and *yz*) are located at  $4675\text{\AA}$  and  $5500\text{\AA}$ , regions of an early-type galaxy’s spectrum that are relatively free of metallicity features, and define a temperature or continuum color index. A third filter (*vz*) is located at  $4100\text{\AA}$ . This region is shortward of the continuum at  $4600\text{\AA}$ , but above the Balmer discontinuity, and is strongly influenced by metal absorption lines (i.e. Fe, CN). While of limited value for young stellar populations, the *vz* – *yz* color is very sensitive to metallicity for spectral classes F to M, that dominate the light in old stellar populations. We parameterize the absolute magnitude of a galaxy to the  $M_{5500}$  luminosity where  $m_{5500}$  is determined by spectroscopic standards taken through our *yz* filter (Rakos, Odell & Schombert 1997). We have converted other studies  $M_V$  or  $M_B$  magnitudes to  $M_{5500}$  using their published  $B - V$  colors (since the  $V$  filter has a slightly higher red side, the conversion from  $M_V$  to  $M_{5500}$  is such that  $M_{5500} = M_V + 0.005(B - V)$ ).

With respect to the CMR, a clear relationship has been demonstrated in all the narrowband filters versus galaxy luminosity, and the resulting correlations are stronger, and with less scatter, than the broadband versions. For cluster early-type galaxies, Odell, Schombert & Rakos (2002) outlined the CMR over a broad range of galaxy absolute magnitudes ( $M_{5500} = -22$  to  $-14$ ) in Coma. The strongest correlation (and steepest slope) is found between *vz* – *yz* color and luminosity. This is in contrast to broadband filters where the strongest correlations are found between near-UV colors (i.e.  $U - V$ ) and stronger than our own near-UV color index, *uz* – *vz*. Our early interpretation is that this confirms a strong metallicity influence on the CMR, for if age was a

significant contributor than the correlation would be stronger in our continuum colors ( $bz - yz$ , Rakos & Schombert 2005).

Since our work in Coma, we have sampled an additional eight rich clusters out to redshifts of 0.17. When combined with our previous work (over the last 25 years), we have a total sample of 1,104 galaxies in the cores of rich clusters (see Rakos & Schombert 2008), and we present the CMR for all 1,104 galaxies in Figure 1. In our previous studies, we have separated the blue and red clusters populations based on a galaxy’s  $bz - yz$  color with blue galaxies being defined as those with a  $bz - yz$  index less than 0.22 (Rakos *et al.* 2000). Division by color ties in a linear fashion with galaxy morphology, where star-forming disk galaxies are easily excluded by this selection criteria (see discussion in Rakos & Schombert 2005b). This division by  $bz - yz$  color is applied in Figure 1 and it is clear that the red population forms a much stronger correlation with luminosity when the blue population is excluded.

The fact that the CMR is a mixture of galaxies with different star formation histories is well known (see Balogh *et al.* 2004). This produces a technical difficulty in using the CMR to interpret galaxy ages and metallicities as any linear (or non-linear) fit to the data will be biased towards the contaminating blue population. Selection criteria using colors introduces a reverse bias (Baldry *et al.* 2004) and selection by morphology also introduces blue galaxies with early-type morphologies (Rakos & Schombert 2005b). Recent studies using massive SDSS datasets can deconvolve the red and blue components of the CMR (Balogh *et al.* 2002) and indicates that the CMR of the red population is not linear with luminosity, thus, making a linear fit to the data inappropriate. This analysis is consistent with the data for the red population in Figure 1.

Our method of choice for understanding the properties of the CMR in our narrowband filters is to parameterize the luminosity/color space with a ridgeline analysis. This procedure divides the total sample in bins of absolute luminosity. Each bin’s distribution of color is then subjected to a gaussian fit to determine a peak color and normalized variance. The peak colors are used to define the ridgeline and this is a robust measure of a maximum value since, if the number of data points is large, the bin size can be varied as an internal measure of the accuracy of the mean color.

The calculated ridgeline for our  $vz - yz$  color is shown in Figure 2. Here the red population (808 galaxies) are displayed greyscale contrast map. This contrast map is produced by assuming that each data point is a 2D gaussian of width given by its photometric error. The individual gaussians are summed and a greyscale intensity per pixel is assigned based on that summation. The pixel grid size is chosen to represent the mean error in color. The ridgeline follows the peak intensities of the greyscale plot, as expected. The CMR ridgeline is roughly linear to within the accuracies of the method. There is no strong indication of upward or downward trends at the bright and faint ends, although there is the suggestion of a flattening at the faint end (see also Baldry *et al.* 2004).

The linear shape of the ridgeline disagrees with the results of Baldry *et al.* (2004) who find, even after separating the red and blue populations in a 70,000 galaxy SDSS sample, that the  $g - r$

CMR is not well fit by a straight line, but rather a linear fit on the high luminosity end with a tanh function at the fainter transition region ( $M_{5500} = -19$ ). Clearly, the difference in sample sizes makes the shape analysis of the SDSS sample superior with our sample. However, our sample is strictly a cluster core sample, the highest galaxy density environment for any evolutionary study. There is every indication that environmental effects vary across regions of differing density (Clemens *et al.* 2008) and across galaxy mass (Hyeop Lee *et al.* 2008). The more linear nature to our CMR may simply reflect the homogeneous nature to evolutionary processes in cluster cores.

To summarize our results on the  $vz - yz$  CMR, we found the following discernible correlations that are relevant to our comparison of a galaxy’s age and metallicity. First, there are clearly two populations involved when a galaxy’s absolute luminosity is compared with its color index. A red population, whose CMR is increasing in color with luminosity and whose colors are indicative of a non-star-forming system, plus a blue population, whose colors indicate recent (last few Gyr) or ongoing star formation. A ridgeline analysis of the red population displays a well correlated relationship between luminosity and color that is, approximately, linear to within the internal errors. The CMR is steepest in our  $vz - yz$  colors, compared with  $uz - vz$  or  $bz - yz$ , which is slightly surprising as the CMR is strongest in the bluest colors for the Johnson  $UBV$  system (Wyder *et al.* 2007). Since  $vz - yz$  is a color sensitive to metallicity effects, this will support a metallicity interpretation to the CMR.

### 3. Interpretation of the CMR

In order to interpret the colors of a galaxy, as they reflect its star formation history, one must consult spectroevolutionary (SED) models (see Schiavon 2007 for a review). These models gather all the relevant star formation information (the assumed IMF, age, metallicity, star formation rate) and output a summed spectrum of the entire underlying stellar population. These spectra can then be convolved through our various filters to produce the narrowband colors that we observe.

In recent years there have been a number of SED models in the literature (Cid Fernandes *et al.* 2008; Franzetti *et al.* 2008; Li & Han 2007; Schulz *et al.* 2002). With respect to our narrowband indices, we have found that most have converged to identical results for stellar populations older than 1 Gyr (see Schombert & Rakos 2009 for a full discussion of the various models and the predicted colors). For this study, we have selected the Bruzual & Charlot (2003, hereafter, BC03) models, although the choice of a particular flavor of models does not change our results.

The BC03 models provide the user with a range of ages (from 0.1 to 20 Gyr) and metallicities (from  $-2.3$  to  $+0.4$  [Fe/H]) for a simple stellar population (SSP), i.e. a stellar population that is singular in age and metallicity. For our purposes, we have selected a fairly standard range of models from 1 to 14 Gyr and  $-2.3$  to  $+0.4$  in [Fe/H], all using the Chabrier (2003) IMF (mass cutoff at 0.1 and  $100 M_{\odot}$ ) and Padova 2000 isochrones. Each SSP is interpolated at the 0.1 dex level in metallicity and convolved to our narrowband filters to produce a full grid of colors. Table 1 lists



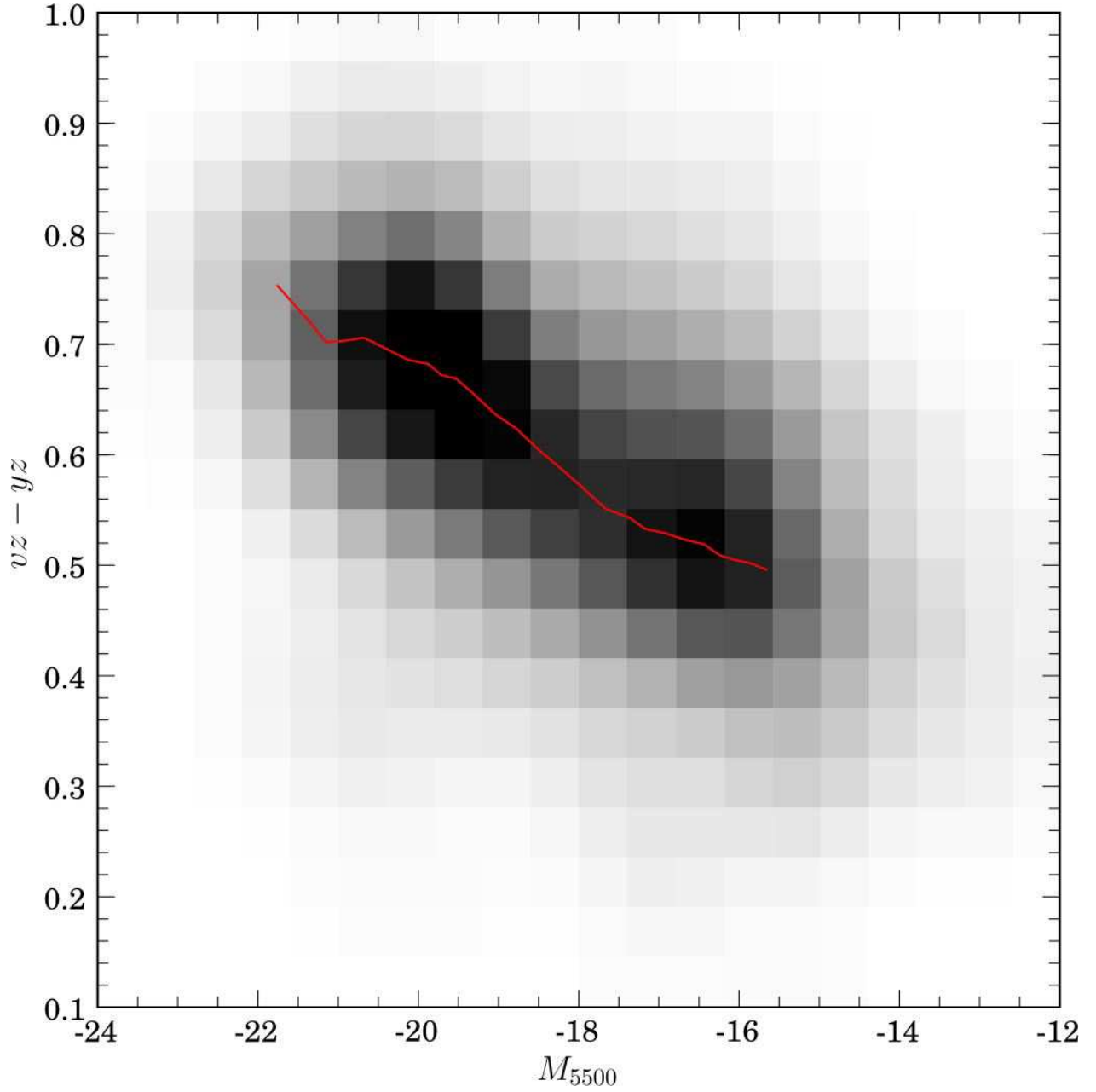


Fig. 2.— A contrast map of the  $vz - yz$  CMR. Each individual data point is treated as a 2D gaussian with its width determined by the photometric errors. All the individual gaussians are summed and binned to produce a greyscale map where intensity represents the data density at that pixel value. The red line represents the ridgeline defined by the gaussian data. The ridgeline is linear to within the errors.

the SSP colors (our narrowband system, Johnson  $U - B$ ,  $B - V$ ,  $V - K$  and the Lick indices  $\langle \text{Fe} \rangle$ ,  $\text{Mgb}$  and  $\text{H}\beta$ ) for two ages, 5 and 12 Gyr. The reddest (i.e. most massive) ellipticals ( $vz - yz = 0.75$  and  $B - V = 0.95$ ) would have higher than solar metallicities for 5 Gyr models and slightly less than solar metallicities for 12 Gyr models.

A more advanced use of SED models is assume that galaxies are not composed solely of SSPs, but rather a sum of SSP's of varying metallicities following a simple chemical evolution model (Schombert & Rakos 2009). These chemical evolution models can take on a range of shapes, as a function of  $[\text{Fe}/\text{H}]$ , dependent on initial conditions and physics input to the models. We have used a simple infall scenario (Kodama & Arimoto 1997) that matches the shape of the internal metallicity distributions for the Milky Way (Wyse & Gilmore 1995), M31 (Worthey *et al.* 2005) and NGC 5128 (Harris & Harris 2000). We have then allowed this metallicity distribution to slide in the peak  $[\text{Fe}/\text{H}]$  value to produce a range total metallicities per galaxy age (see our ‘push’ model, Schombert & Rakos 2009). We argue in that study that this model matches the  $\langle \text{Fe} \rangle$  versus color plane but, again, the exact shape of the adopted metallicity distribution is not a key parameter to our following conclusions.

Each model produces a metallicity value based on a sum of the model metallicity bins (a numerical average) and a luminosity weighted value (metal-poor stars are hotter, and therefore brighter, than metal-rich stars). The difference between these values has a minor correction as outlined in Schombert & Rakos (2009), in other words, it is easy to convert between the two values. In our following analysis, we always use the luminosity-weighted  $[\text{Fe}/\text{H}]$  values. Examples of our multi-metallicity model results are listed in Table 1. Our 5 and 12 Gyr model (for  $[\text{Fe}/\text{H}]$  values from  $-2$  to  $+0.8$ ) is shown in Figure 3, a two color diagram ( $vz - yz$  versus  $bz - yz$ ) for our cluster sample. The 12 Gyr model agrees well with the ridgeline of the data; however, a large range of ages would equally satisfy the data and this diagram is a poor indicator of mean age and metallicity (Rakos & Schombert 2004). We present this plot to demonstrate the models span the same range of color space as the observations. We also note that the accuracy of the models is limited by the accuracy of the input age and metallicity values. Typical errors quoted for age and  $[\text{Fe}/\text{H}]$  in the literature are 0.5 Gyr and 0.2 dex (Rakos & Schombert 2005). These variations map into a model color error for  $vz - yz$  of 0.01 and 0.06 respectfully. These are similar to the photometric errors for the faint end of our cluster samples and, thus, we do not expect to be model limited in our interpretations.

There are several features to note in Table 1 with respect to comparing our multi-metallicity models with SSP's. First, for the same mean  $[\text{Fe}/\text{H}]$ , the multi-metallicity models produce bluer colors ( $-0.13$  in  $\Delta(vz - yz)$ ,  $-0.04$  in  $\Delta(B - V)$ ,  $-0.05$  in  $\Delta(V - K)$ ) than their equivalent SSP models. This is due, of course, to the inclusion of a metal-poor tail that contributes more strongly to color than mean  $[\text{Fe}/\text{H}]$ . For our multi-metallicity models, red ellipticals would only have solar and higher metallicity for ages greater than 10 Gyr. Younger models would require super-solar metallicities to explain the colors of the brightest ellipticals, values that are inconsistent with  $\langle \text{Fe} \rangle$  values (between 2.3 and 3.0). Whereas, the older multi-metallicity values have metallicity

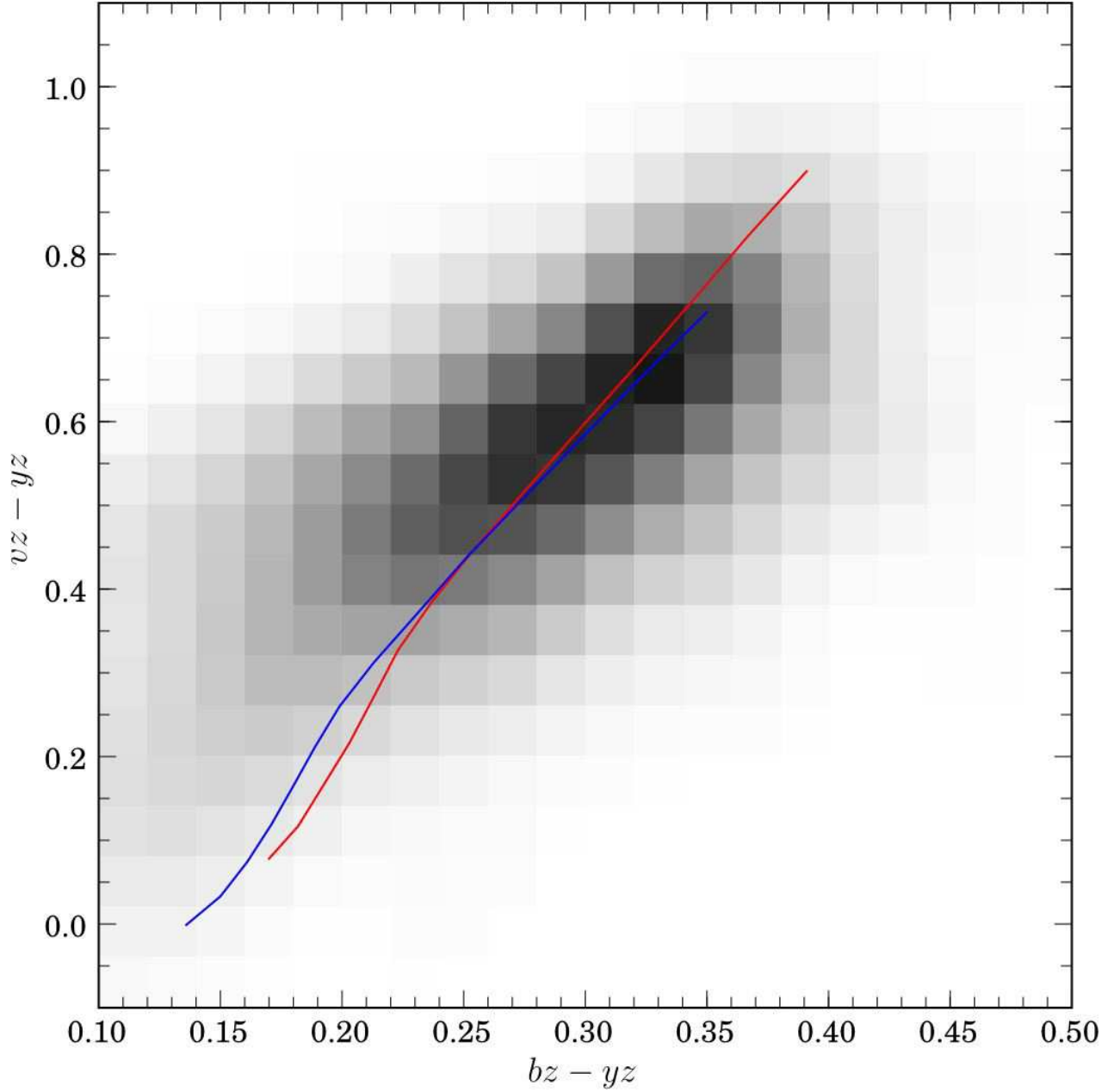


Fig. 3.— The two color diagram, our metallicity color,  $vz - yz$ , versus our continuum color,  $bz - yz$ . The correlation between colors is well known (Rakos & Schombert 2007). The red line is a 12 Gyr multi-metallicity model (see discussion), the blue line is a 5 Gyr model. Either is an adequate description of galaxy colors, although the younger models require super-solar metallicities for the reddest ellipticals.

indices,  $\langle \text{Fe} \rangle$  and  $\text{Mgb}$ , in agreement with the colors of bright ellipticals. High  $\text{H}\beta$  values, i.e. greater than 2, are a challenge for older multi-metallicity models as they predict extremely blue colors. This will be discussed further in §5.

Lastly, we need to consider the effects of  $\alpha$ -enhancement to the SED models. It has been known for some time that massive early-type galaxies are enhanced in light elements (so-called  $\alpha$  elements, see Worthey *et al.* 1992) compared with Fe. SED models that use varying ratios of  $\alpha/\text{Fe}$  will predict differing colors, mostly due to variations in the effective temperature of the RGB. Thomas *et al.* (2005) find  $[\alpha/\text{Fe}]$  varies from 0 to 0.3 in cluster ellipticals. This agrees well with Trager *et al.* (2008)  $\text{Mg}/\text{Fe}$  ratios in Coma. For our models, we consider the changes in color ( $B - V$ ) presented for the  $[\alpha/\text{Fe}] = +0.3$  from Schiavon (2007) and Percival *et al.* (2009). For those models, with ages greater than 5 Gyrs, it is found that  $B - V$  reddens by 0.02 between the solar and  $\alpha$ -enhanced models. This translates into  $\Delta(vz - yz) = 0.03$  for our color system, and will be our baseline for comparison in §4. As the  $vz$  filter is centered on a region of the spectrum (4600Å) rich in metallicity lines, it is possible that  $\alpha$  enhanced models will deviate  $vz - yz$  redward to a greater degree than  $B - V$ . However, as most of the differences are due to RGB temperatures, not line blanketing effects, we assume that a change of 0.03 is a reasonable approximation for  $\alpha/\text{Fe}$  variations.

While our narrowband color system is an improvement over broadband colors in discriminating age and metallicity (see Rakos & Schombert 2005 and Rakos & Schombert 2007), there is still a degeneracy in going from color to age and metallicity. However, it is the nature of the underlying stellar population that the two parameters of age and metallicity define a unique color. Thus, we can use the SED models to deduce the expected colors of galaxy's with age and metallicity values determined in another fashion, in this case, spectroscopically.

#### 4. Spectroscopic Ages

Attempting to extract age and metallicity from galaxy colors is a difficult procedure with a great deal of internal error associated with the well known age-metallicity degeneracy problems (see Rakos & Schombert 2005). However, in order to test the validity of spectroscopic age and metallicity determinations, we need only use the observed spectral index age and metallicity values and calculate their expected narrowband colors. Where a set of galaxy colors may be due to a range of ages and metallicities, a couplet of age and metallicity values has only a singular set of corresponding colors. Thus, this procedure depends only on the accuracy of the SED models and produces a unique set of colors without degeneracy.

Using the multi-metallicity SED models from §3, and the luminosities, ages and metallicities listed in Trager *et al.* (2008) and Thomas *et al.* (2005), we can calculate the expected colors and plot these values on the  $vz - yz$  CMR (a galaxy's total luminosity is independent of the models). This experiment is shown in Figure 4, where the blue symbols are from the Trager *et al.* sample

and the green symbols are from the Thomas *et al.* sample. The greyscale image is our cluster data and the red ridgeline taken from Figure 2. It is immediately obvious that neither dataset matches the CMR for cluster galaxies. For the combined Trager *et al.* and Thomas *et al.* datasets, 97% of their galaxies lie below (i.e., having bluer colors) the ridgeline. While the predicted colors are not outside the range of galaxy colors for the entire sample (e.g., the lower luminosity galaxies), they are significantly bluer than galaxies of similar absolute luminosity. Both Trager *et al.* and Thomas *et al.* samples are dominated by high mass galaxies ( $M_{5500} < -19$ ), but there is no evidence that colors for the low mass end of the sample are closer to the CMR than those on the high mass end.

The magnitude of the difference between the spectroscopic colors and the CMR, as a function of absolute luminosity, is shown in Figure 5. Shown in this Figure is the difference between the model color (from the spectroscopically determined age and metallicity) and the CMR ridgeline (the scatter around the ridgeline is 0.08). The dotted red line is the mean color difference for the sum of all three samples, which is 0.12 mags blueward of the CMR. There is no correlation between color separation from the CMR and luminosity (stellar mass). Also shown are the errors in model color due to errors in the age and metallicity estimates. Neither error is sufficient to explain the discrepancy in color. Also shown is the color effect of assuming a different  $\alpha/\text{Fe}$  ratio (which reddens color for a given age and metallicity, see discussion in the previous section).

As a secondary check to our procedures, over a larger range in luminosity, we have taken the linear relationships between galaxy mass, age and metallicity from the early-type Gallazzi *et al.* (2006) SDSS sample (see their Table 4) and calculated  $vz - yz$  colors for that set of ages and metallicities. Although these relations, quoted in Gallazzi *et al.* Table 4 are linear, they, in fact, predict increasing  $[\text{Fe}/\text{H}]$  with increasing age, in contradiction with their Figure 18. This simply reflects the spread in  $[\text{Fe}/\text{H}]$  per stellar mass bin (see their Figure 17). To better represent the SDSS dataset, we have outlined a region in color space that marks the boundaries for  $[\text{Fe}/\text{H}]$  (from their Figure 17, an  $[\text{Fe}/\text{H}]$  range of  $-0.2$  to  $+0.1$  at a mass of  $10^{9.75}$  and a range of  $0.0$  to  $+0.3$  at a mass of  $10^{11.5}$ ) and adopts the linear relation of age and stellar mass. To convert stellar mass into  $M_{5500}$  we have adopted the relationship between  $M_r$  and  $M_*$  from Table 4 of Gallazzi *et al.* (2006) ( $M_r = -2.29\log M_* + 3.45$ ) and assuming  $V - r = 0.30$  from SDSS transforms for a mean color of  $g - r = 0.75$ .

That experiment is shown in Figure 6 where the relationships from Gallazzi *et al.* age and metallicities are converted into  $vz - yz$  colors. As with the Trager *et al.* and Thomas *et al.* samples, the Gallazzi SDSS sample also lies below the CMR ridgeline, a closer match at the low mass end where galaxies have spectroscopic ages of 7 Gyrs and mean  $[\text{Fe}/\text{H}]$  of near solar. The colors of the high mass end are bluer than the observed CMR, although not as dramatic as the Thomas *et al.* and Trager *et al.* samples. This problem is also noted if we use their age and metallicity to predict SDSS colors ( $g - r$ ) (see Gallazzi *et al.* (2006), Figure 4) or Johnson  $UBV$  colors. We also note that applying any correction for  $\alpha$ -enhancement would only redden the predicted colors by 0.03 (see discussion in previous section), which is insufficient to explain the discrepancies in Figures 5 or 6.

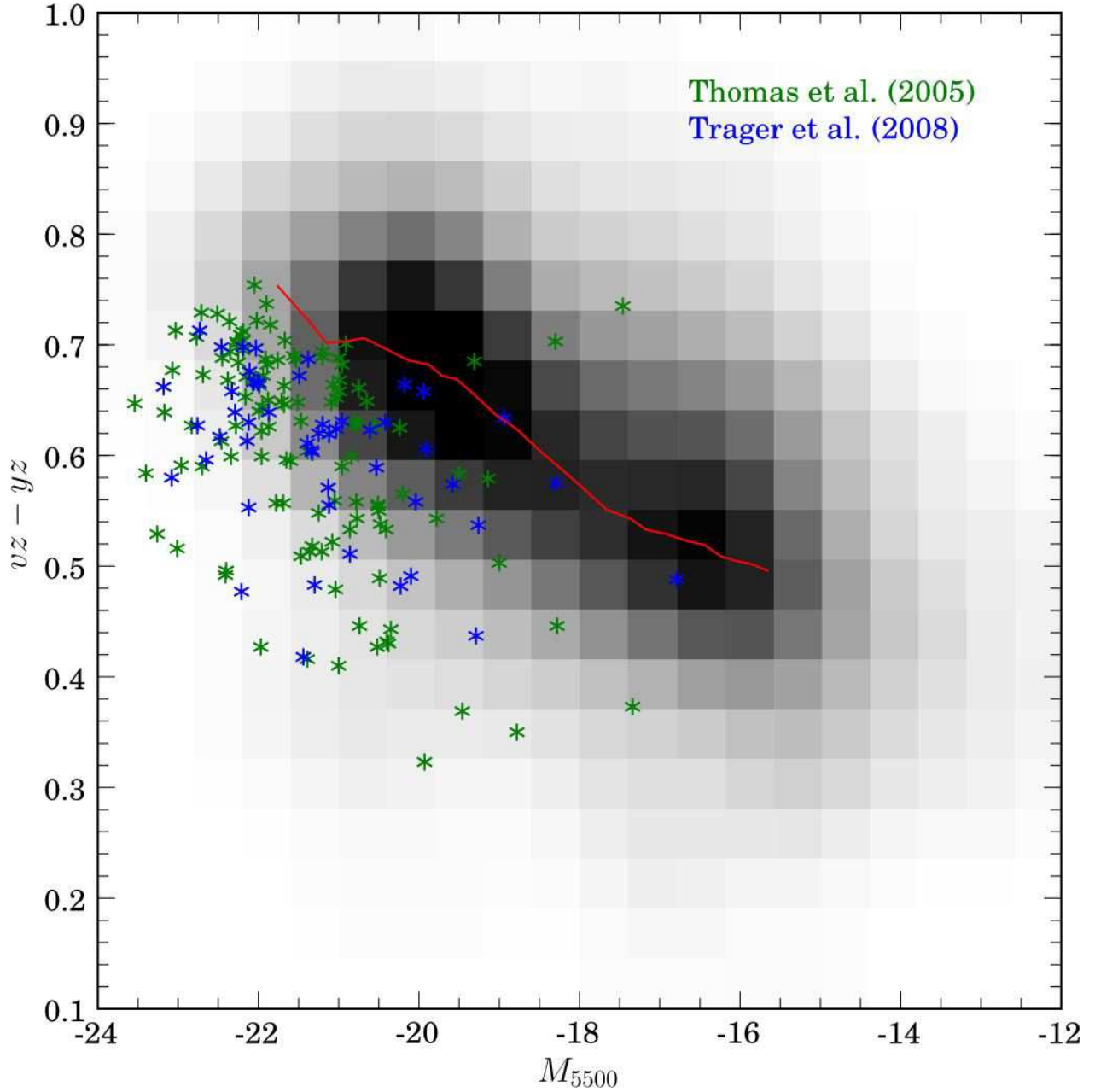


Fig. 4.— The calculated  $vz - yz$  colors for the samples of Thomas *et al.* (2005) (green symbols) and Trager *et al.* (2008) (blue symbols). The spectroscopic ages and metallicities from those studies are used to calculate their  $vz - yz$ , and then plotted against  $M_{5500}$  absolute magnitude. Our  $vz - yz$  cluster data and ridgeline (red line) from Figure 2 are also shown. A majority of the spectroscopic data lie blueward of the  $vz - yz$  CMR indicating that the spectroscopically measured age and/or metallicity values are in error.

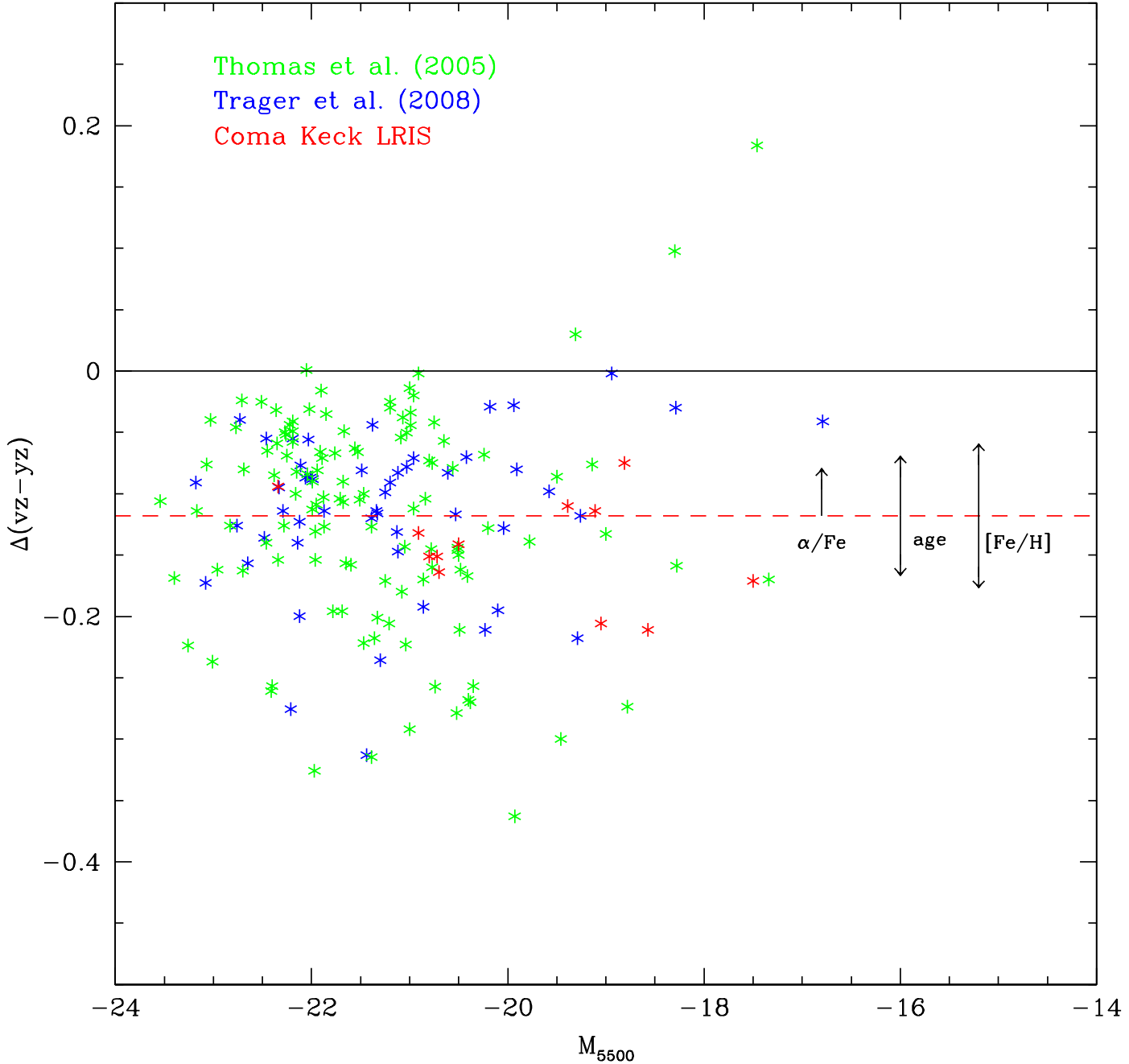


Fig. 5.— The difference between the model colors (as given by spectroscopic age and metallicity) and the CMR ridgeline from Figure 4. Both Trager *et al.* and Thomas *et al.* samples are shown, as well as the high S/N Keck sample (Trager *et al.* 2008) of bright galaxies in Coma. The red dotted line is the mean color difference for the samples. The age and  $[\text{Fe}/\text{H}]$  arrows display the spectroscopic errors for age and metallicity as they reflect into model color. Also shown is the shift in color needed to correct for enhanced  $\alpha/\text{Fe}$  models. None of the errors or corrections approach values needed to explain away the discrepancy with the CMR.

It only remains to determine which parameter, age or metallicity, is responsible for the deviations from the CMR. The obvious candidate is stellar population age since the difference is in the direction of bluer colors, and ages less than 8 Gyr have a larger impact on optical color than metallicity. In addition, the metallicities quoted by all three spectroscopic studies are in fair agreement with direct metallicity measurements based on high resolution imaging of nearby galaxy’s CMD’s (Worthey *et al.* 2005). In order to redden the colors of either the Trager *et al.* , Thomas *et al.* or Gallazzi *et al.* samples using solely changes in metallicity (in order to maintain their young ages) would require increasing their mean  $[\text{Fe}/\text{H}]$  to super-solar values, in conflict with the metallicity of the Milky Way and other Local Group galaxies where metallicity is determined directly through CMD diagrams. Ages of 5 to 7 Gyr for low mass ( $10^9 M_{\odot}$ ) galaxies can be preserved, but require solar metallicity values, in contradiction with the spectroscopic studies own  $[\text{Fe}/\text{H}]$  estimates (although the SDSS samples display a large range in metallicity at the low mass end).

In order to test the hypothesis that age is primarily responsible for the deviations in Figures 5 and 6, we have re-calculated all the colors for the three samples using the spectroscopic metallicity values, but assuming a mean age of 12 Gyr rather than the spectroscopically determined age. We note that since age and metallicity are determined from the  $\text{H}\beta/[\text{MgFe}]$  diagram, and lines of constant metallicity are nearly vertical in this diagram, there is only a small correction to the calculated metallicity from the MgFe index if a galaxy’s age is increased. This correction is in the direction of decreasing the total metallicity (bluer colors) and has the magnitude of approximately 0.2 dex from 12 to 7 Gyr. Interestingly, this correction is balanced by difference between a metallicity determined by SSP’s versus a luminosity weighted value for  $[\text{Fe}/\text{H}]$  from a stellar population that has a range of metallicities (this correction increases the mean  $[\text{Fe}/\text{H}]$  by 0.25 dex, see Schombert & Rakos 2009). This balance may explain why the spectroscopic  $[\text{Fe}/\text{H}]$  values for galaxies agrees with other techniques, while underestimating a galaxy’s mean age.

The age corrected data points are shown in Figure 7. Using an old stellar age, we find that both the Trager *et al.* and Thomas *et al.* data are well matched to the CMR, and the slope of the CMR is completely determined by changes solely in mean metallicity with galaxy mass. The excellent match for the corrected data is slightly deceiving as it is assisted by the fact that there is a correlation between age and metallicity in the Thomas *et al.* and Trager *et al.* samples in the sense that the oldest galaxies have the lowest metallicities. Their reddest galaxies (with ages greater than 12 Gyrs) have the lowest metallicity and lie only slightly below the ridgeline. Correcting these colors to 12 Gyrs moves them only slightly bluer. Galaxies with the youngest ages have the highest metallicity, and correcting their colors to a 12 Gyr age places them above the ridgeline (on average) due to their higher  $[\text{Fe}/\text{H}]$  values. However, the mean effect for the corrected sample is valid, correcting young ages to 12 Gyrs reddens their colors by an amount that places them in agreement with the CMR.

In addition, we have corrected the Gallazzi *et al.* relationship to 12 Gyr, also shown in Figure 7. The resulting region is an excellent match to the CMR ridgeline in both  $vz - yz$  and  $g - r$  (not shown), at the low mass end, but slightly flatter than the observed CMR. The Gallazzi *et al.* region



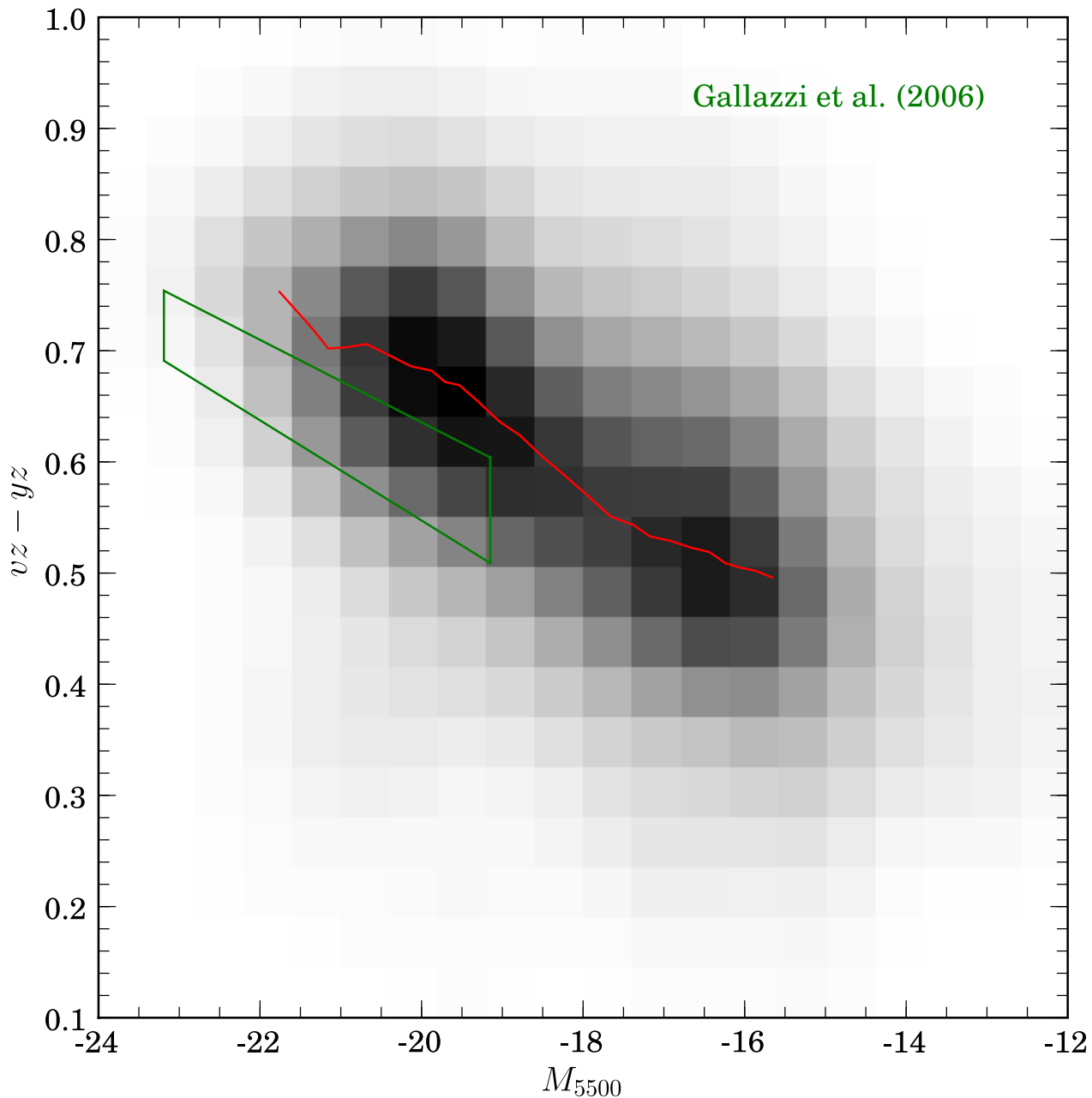


Fig. 6.— The calculated  $vz - yz$  colors for the SDSS sample of Gallazzi *et al.* (2006). We have used their derived bounds for age and metallicity (their Table 4, green polygon) to calculate  $vz - yz$  color. As with Thomas *et al.* and Trager *et al.* samples, the SDSS mean values all lie blueward of the mean CMR (red line), although achieve a better match as low masses.

also nicely brackets the corrected Trager *et al.* and Thomas *et al.* samples. The corrected region is slightly lower for the high mass end ( $M_{5500} < -22$ ). To within the accuracy of the measurements, and our technique, we find that high luminosity early-type galaxy's color can be reproduced by assuming old ages ( $\tau > 12$  Gyr). In addition, the corrected colors match the CMR such that there is no evidence of a significant population of galaxies younger than 10 Gyr, at least for luminosities greater than  $-19$ .

As a last check to our technique we have examined the high resolution data from the Coma cluster core galaxy by Trager *et al.* (2008). This dataset represents the highest quality spectroscopic indices to date and is analyzed to dismiss any debate that spectroscopic ages and metallicities are inherently inaccurate. The resulting age and metallicities for the sample are listed in Table 5 of Trager *et al.* (2008). They range from 3.0 to 9.2 Gyr and  $-0.25$  to  $+0.54$  in  $[\text{Fe}/\text{H}]$ . Narrowband colors were obtained for these galaxies in Odell, Schombert & Rakos (2002). Model colors ( $vz - yz_{model}$ ) versus observed colors are shown in Figure 8, where we generated model colors using the Trager *et al.* (2008) ages and metallicities (black labels). Again, we see that the predicted model colors are bluer than the observed colors. And, again, we calculate new model colors using an age of 12 Gyr and  $[\text{Fe}/\text{H}]$  values determined strictly from the  $\langle \text{Fe} \rangle$  index (Schombert & Rakos 2009). These values are shown as red symbols in Figure 8, and as our previous results we find the new colors in excellent agreement with the observed colors (the one-to-one line is shown in blue for Figure 8).

We can reverse our previous arguments with the Coma data by holding the metallicity fixed at some particular value (e.g. solar) and use the spectroscopic ages to determine the colors. This experiment is shown in Figure 8 as the green symbols where all the metallicities were assumed to be solar. The metallicity data is a poor match to the observations, and a fixed metallicity is clearly wrong given the variations in  $\langle \text{Fe} \rangle$ . However, if one uses the spectroscopic ages, and increases the  $[\text{Fe}/\text{H}]$  value for each galaxy to match the observed colors, then all the Coma galaxies require a mean increase in  $[\text{Fe}/\text{H}]$  of  $+0.5$  dex, ranging from solar for the low mass galaxies to  $+0.8$ . However, these values disagree with other metallicity indicators in cluster galaxies (Graves & Schiavon 2008).

Our analysis in Figure 8 differs from our previous technique by using the  $\langle \text{Fe} \rangle$  to determine  $[\text{Fe}/\text{H}]$  in a model independent fashion. This leaves age as the sole independent parameter and, again, an old stellar age is required to reproduce the observed colors. The importance of the Trager *et al.* Keck data is that it is clear that the younger age estimates from the spectroscopic data are driven by high  $\text{H}\beta$  values for the data is of such a high quality there is little uncertainty to their measured values. And there can be no doubt from the Keck data that the  $\text{H}\beta$  values for all the Coma galaxies are greater than expected for any standard model of a 12 Gyr population (see Table 1). Therefore, the dilemma for any SED model is to reproduce the  $\text{H}\beta$  values measured by numerous spectroscopic surveys and SDSS samples, yet maintain red continuum colors (from the near-UV to the near-IR) for the galaxy as a whole.

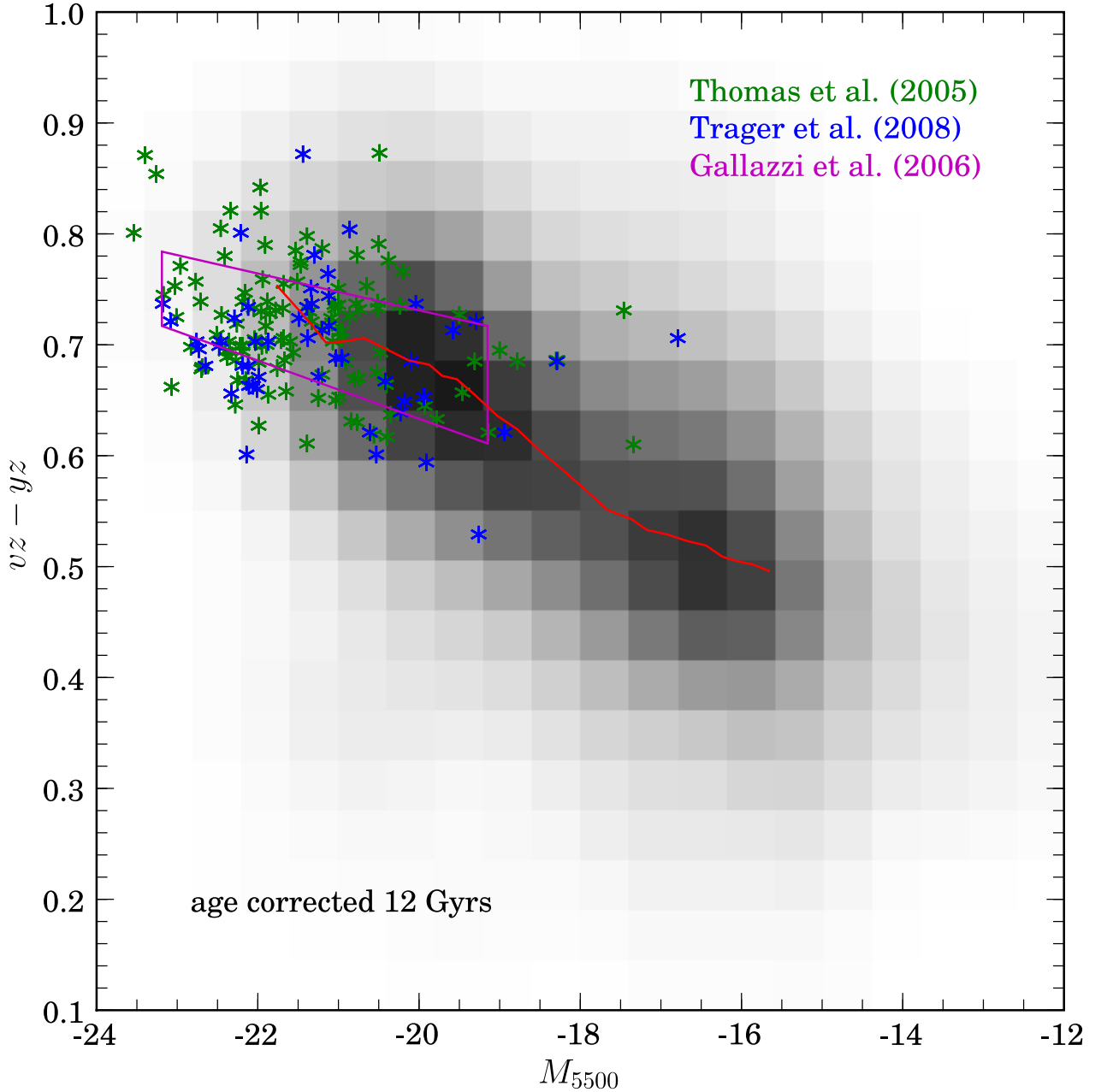


Fig. 7.— The age corrected CMR for all three spectroscopic samples. These are the same samples as Figures 5 and 6; however, the galaxy colors are calculated using an assumed age of 12 Gyr rather than the spectroscopically determined ages. The spectroscopically determined metallicity values are used, although an older age would imply slightly lower  $[\text{Fe}/\text{H}]$  values as calculated from metallicity indices such as  $\text{MgFe}$ . All three spectroscopic samples are now in agreement with the CMR.

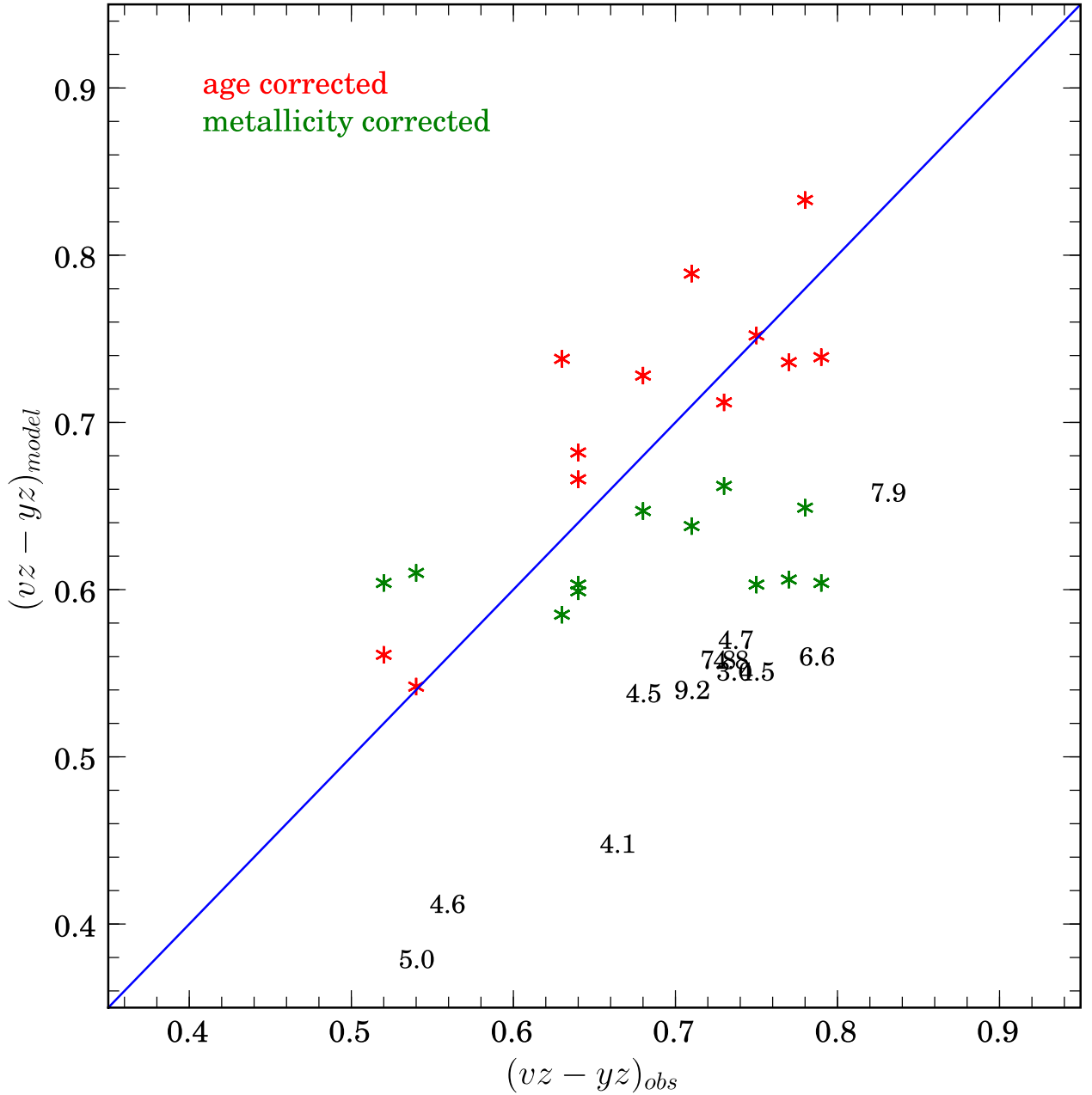


Fig. 8.— The Coma Keck spectroscopic sample from Trager *et al.* (2008). This sample represents the highest quality spectral indices for age and metallicity determination to date. The black symbols are the observed narrowband  $vz - yz$  colors (Odell, Schombert & Rakos 2002) versus their model colors using spectroscopic age and metallicity values. The galaxies spectroscopic ages are shown. The red symbols display the same galaxies with model colors assuming an age of 12 Gyr and metallicity determined solely from the  $\langle \text{Fe} \rangle$  index. The green symbols represent the same analysis, only using the spectroscopic ages, but fixing the metallicity to solar values.

## 5. Narrowband Colors and $H\beta$

While all indications are that age is primarily responsible for problems with the spectroscopic samples, there is no clear understanding for why this is the case. A stellar population’s age is determined, primarily, from its  $H\beta$  index. The spectroscopic studies considered herein deduce age from the MgFe versus  $H\beta$  diagram using similar models from which we extract our narrowband colors. In fact, for the Coma sample, one can use the MgFe and  $H\beta$  values to reproduce the metallicity and ages in Trager *et al.* (2008), so model interpretation is not the central problem. In particular, even for multi-metallicity models (Schombert & Rakos 2009), old galaxies have  $H\beta$  values around 1.4, while a majority of normal, early-type galaxies have  $H\beta$  greater than 1.4 (Cervantes & Vazdekis 2008), indicative of ages less than 5 Gyr from the same SED models.

There are several scenarios to increase the  $H\beta$  signature in an old population. However, all of them require the inclusion of a hot stellar component that results in bluer colors, both in broadband and narrowband systems. For example, increasing the number of metal-poor stars in a galaxy will increase the  $H\beta$  index through increases in temperature of the RGB. A first order estimate, based on numerical experiments with SED models, finds a change in  $H\beta$  from 1.4 to 1.6 produces a decrease (bluer)  $uz - yz$  color of 0.16 based on a 10% increase in the number of metal-poor stars ( $[Fe/H] < -1.5$ ). This shift would be in disagreement with the mean colors of the CMR.

Other exotic populations with strong  $H\beta$  signatures (blue stragglers, blue horizontal branch stars, hot white dwarfs) all suffer from the same effect of bluer continuum colors with shifts between  $-0.25$  and  $-0.40$  to the blue for changes of only 0.2 in  $H\beta$ . None of these changes in color are consistent with the CMR.

Introducing young, massive stars is slightly more successful than the previous two experiments. This technique involves mixing a younger stellar population with an older (12 Gyr) population, referred to as ‘frosting’ models (Trager *et al.* 2000). For our analysis we have mixed a 1 Gyr population with our multi-metallicity models of 12 Gyrs. Figure 9 displays the Trager *et al.* (2008) Coma data with our 12 Gyr model and a 10% frosting model (note: this mixture results in a spectroscopic age of approximately 2 Gyrs), plotting our metallicity ( $uz - yz$ ) and continuum color ( $bz - yz$ ) versus the  $H\beta$  and  $\langle Fe \rangle$  indices. The 12 Gyr models are an excellent fit to our colors versus  $\langle Fe \rangle$ ; however, fail to match the  $H\beta$  values. The frosting models increases the  $H\beta$  values, but, as expected, also decrease the colors and fail to match the data. It is instructive to note that the multi-metallicity 12 Gyr model matches the  $\langle Fe \rangle$  versus color data; whereas, the 12 Gyr SSP is a lesser fit to the data and all the frosting models fail to match the  $\langle Fe \rangle$  versus color data.

Another consideration is the effect of higher  $\alpha/Fe$  models on the  $H\beta$  diagrams. As noted in §3, SED models with higher ratios of the  $\alpha$  elements (e.g. Mg) will have slightly redder colors than solar models of the same  $[Z/H]$ . Likewise,  $\alpha$ -enhanced models will have lower  $\langle Fe \rangle$  indices than solar models for a constant  $[Z/H]$ . This effectively raises the  $H\beta$  value per  $[Fe/H]$  value estimated from  $\langle Fe \rangle$ . We estimated, in section §3, that increased  $[\alpha/Fe]$  values of +0.3 (typical for bright ellipticals, Thomas *et al.* 2005), would lead to an increase in  $uz - yz$  of 0.03 (see Figure 5) and

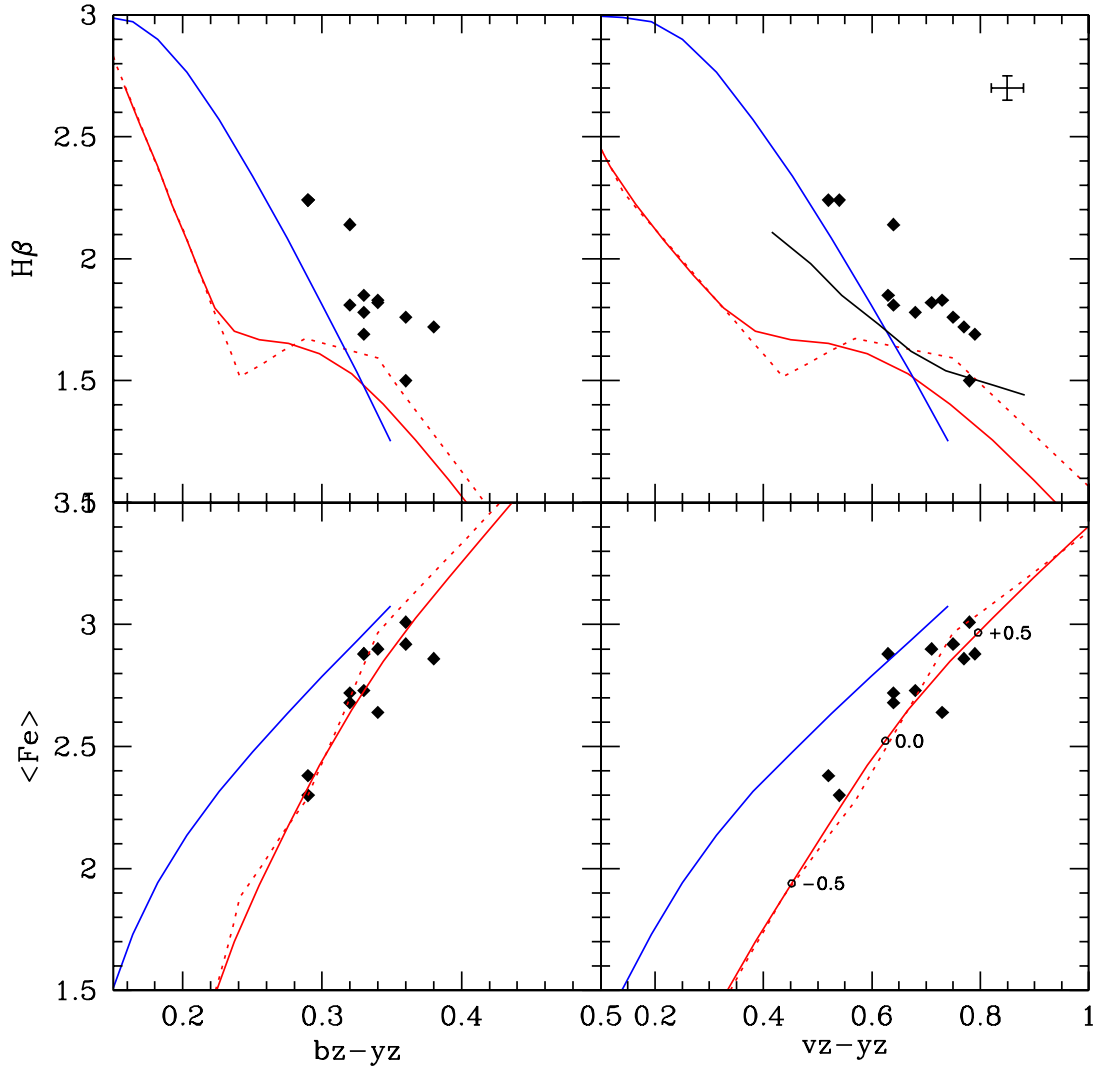


Fig. 9.— The Trager *et al.* (2008) Coma data combined with our metallicity ( $vz - yz$ ) and continuum ( $bz - yz$ ) colors. The solid red line is our multi-metallicity 12 Gyr model ( $[\text{Fe}/\text{H}]$  values are indicated), the dashed red line is a Bruzual & Charlot 12 Gyr SSP. The blue line is a ‘frosting’ model, a 10% 1 Gyr population added to the 12 Gyr model. None of the models adequately match the  $H\beta$  values; however, the multi-metallicity 12 Gyr model is an excellent fit to the  $\langle \text{Fe} \rangle$  versus color diagram, superior to the SSP models. The black solid line represents the  $\alpha$ -enhanced models of Idiart *et al.* (2007).

an increase in  $H\beta$  of 0.2. This is insufficient to explain the discrepancies in Figure 9, but is in the correct direction. For comparison, we plot the  $\alpha$ -enhanced models of Idiart *et al.* (2007) in Figure 9. Again, these models are in the correct direction to resolve the disagreement between models and the data, but fail to predict the magnitude of the  $H\beta$  index.

One important point to extract from Figure 9 is the strong correlation between color and the  $H\beta$  index. For most spectroscopic studies (e.g. Thomas *et al.* 2005), this correlation has been interpreted as reflecting decreasing mean age with decreasing galaxy mass. However, if we accept old, and coeval, ages for ellipticals, then the color- $H\beta$  relation must signal a dependence between metallicity and  $H\beta$  that is stronger than the expected increase in  $H\beta$  due to an increase in the RGB effective temperature with lower metallicity. Again, one might be inclined to invoke a ‘2nd parameter’ problem for galaxy spectra where lower metallicities involve a complex mix of blue horizontal branch stars. However, as discussed above, this does not resolve the lack of bluer continuum colors that such a population would express.

## 6. Conclusions

Using a narrowband color system, we have examined the impact of the deduced younger ages for early-type galaxies in clusters proposed by numerous spectroscopic surveys under the Lick system. The color-magnitude diagram is the tool of choice for testing SED model colors as one axis (magnitude) is limited in its explanation (i.e., galaxy stellar mass) leaving only galaxy color as open for interpretation.

We summarize our results as follows:

- The CMR for our narrowband color system is well defined and consistent with the known changes in broadband colors. The slope is steepest for the  $vz - yz$  ‘metallicity’ color, that also has the lowest internal errors and intrinsic scatter.
- SED models have reached a level of sophistication that now allow for detailed testing of integrated colors as a function of age and metallicity. However, as expected, a range of model parameters (in terms of stellar population age and metallicity) can reproduce the various color-color diagrams in our filter system. Of course, the converse is not true, a pair of age and metallicity values will correspond to a unique galaxy color. We can use this effect to test the integrity of ages and metallicities determined by spectroscopic values by comparing predicted model colors with a one parameter relation such as the CMR. As these models contain the same assumptions and calculations as the models in which the spectroscopic groups use to convert their indices into age and metallicity, then the results should be the same.
- Converting the ages and metallicities from the Trager *et al.* (2008) and Thomas *et al.* (2005) spectroscopic samples into colors, then comparing them to the observed CMR, demonstrates

that spectroscopically determined ages are sharply discordant with CMR (see Figure 5). This discrepancy is visible in all colors (broadband and narrowband), but has the strongest signature in our narrowband system, mostly due to the high sensitivity to metallicity and age effects in our narrowband system and the fact that our colors bracket the region of a galaxy’s spectrum containing the  $H\beta$  feature. Most importantly, this discrepancy is resolved if model ages of 12 Gyr are assumed (see Figure 7). Using spectroscopic ages, yet varying metallicity, requires unrealistic super-solar global metallicity values for galaxies.

- Any possibility that inaccurate spectroscopic values are responsible for young ages is removed when the high resolution Keck data for Coma is considered (Trager *et al.* 2008). This dataset has the highest S/N of any spectroscopic survey, particularly for the critical  $H\beta$  index, and still display the same inconsistent colors for a stellar population of assumed young age (see Figure 8).
- On the other hand, using the same Coma data, with matching narrowband colors, finds excellent agreement between spectral indices, such as  $\langle Fe \rangle$  and colors. The conflict only arises between the  $H\beta$  index and colors. There is a strong correlation between  $H\beta$  and color (bluer colors result in higher  $H\beta$  values); however, none of our experiments to add a hot stellar component to an underlying old stellar population can raise the SED  $H\beta$  values without introducing discordant blue colors.

We are left with the conclusion that the unusual aspect to ellipticals is not a young stellar age, but rather their high  $H\beta$  values without a significant hot component to their underlying stellar population to explain these values. And our numerical experiments demonstrate that if you adopt  $\langle Fe \rangle$  values calibrated to  $[Fe/H]$  then you can reproduce the CMR with no need for galaxy mean ages of less than 10 Gyr. There are only two possible interpretations for this dilemma, either 1) the  $H\beta$  index is incorrectly interpreted and the galaxies are composed of old (greater than 10 Gyr) stellar populations to match their colors and metallicities as given by metal indices or, 2) our SED models correctly map the  $H\beta$  values into age-metallicity space and the spectroscopic results are correct, i.e., many galaxies have young stellar populations, but then the SED models incorrectly predict all narrowband and broadband colors.

Nearly every spectroscopic study of ellipticals has revealed a significant fraction with large  $H\beta$  indices (greater than 1.6) which implies a young mean stellar population age through interpretation by the most basic SED models (Cervantes & Vazdekis 2008; Caldwell, Rose & Concannon 2003). However, galaxies with ages less than 8 Gyr would challenge our understanding of passive color evolution of galaxies at intermediate redshifts (Rakos & Schombert 1995). While galaxy colors redden quickly and stabilize after 8 Gyrs (Rakos, Schombert & Odell 2008), ages less than 8 Gyrs, as seen in many spectroscopic studies, are impossible to reconcile with the observed colors at redshifts of 0.2 to 0.4. For example, Rakos & Schombert (2005) find the colors of A2218 ( $z=0.18$ ) are consistent with a lookback time of 2 Gyr. However, if the mean ages from the spectroscopic



study of Coma are extrapolated to A2218, the mean colors would be 0.2 mags bluer than those observed.

This has serious consequences to current state of our field of galaxy evolution as every spectroscopic study of galaxies using the Lick system has, therefore, incorrectly deduced galaxy age. This ranges from individual spectroscopic surveys (e.g. Smith *et al.* 2007; Sanchez-Blazquez *et al.* 2006) to large SDSS programs (e.g. Clemens *et al.* 2008). As these age datasets are used to test our galaxy formation scenarios, a great deal of our conclusions on the star formation history of ellipticals is in error.

*Note on astro-ph version:* This version of our work released on astro-ph deviates slightly from the version that will be published. This is due to, what we believe, is a repressive editorial policy that allows an anonymous referee to replace our conclusions to match their personal views. Thus, we have restored several sections of text to re-enforce, more strongly, our results based on our data. Since no one ever references our work, we find the possible confusion in bibliography's to be moot.

Financial support from Austrian Fonds zur Foerderung der Wissenschaftlichen Forschung and NSF grant AST-0307508 is gratefully acknowledged. We also acknowledge all the telescope time granted this project from NOAO (north and south), as well as ESO. This research has made extensive use of the NASA/IPAC Extragalactic Database (NED) which is operated by the Jet Propulsion Laboratory, California Institute of Technology, under contract with the National Aeronautics and Space Administration. Funding for the SDSS and SDSS-II has been provided by the Alfred P. Sloan Foundation, the Participating Institutions, the National Science Foundation, the U.S. Department of Energy, the National Aeronautics and Space Administration, the Japanese Monbukagakusho, the Max Planck Society, and the Higher Education Funding Council for England.

## REFERENCES

- Andreon, S., Puddu, E., de Propris, R., & Cuillandre, J.-C. 2008, MNRAS, 385, 979
- Andreon, S. 2003, Ap&SS, 285, 143
- Bahcall, N. A. 1999, in Mourão, A. M., Pimenta, M. & Sá, P., eds, New Worlds in Astroparticle Physics II, World Scientific Publishers, 77
- Baldry, I. K., Glazebrook, K., Brinkmann, J., Ivezić, Ž., Lupton, R. H., Nichol, R. C., & Szalay, A. S. 2004, ApJ, 600, 681
- Baldry, I. K., Balogh, M. L., Bower, R. G., Glazebrook, K., Nichol, R. C., Bamford, S. P., & Budavari, T. 2006, MNRAS, 373, 469
- Balogh, M. L., Smail, I., Bower, R. G., Ziegler, B. L., Smith, G. P., Davies, R. L., Gaztelu, A., Kneib, J.-P. & Ebeling, H., 2002, ApJ, 566, 123

- Balogh, M. L., Baldry, I. K., Nichol, R., Miller, C., Bower, R., & Glazebrook, K. 2004, *ApJ*, 615, L101
- Bernardi, M. *et al.* , 2003, *AJ*, 125, 1866
- Bower, R. G., Lucey, J. R., & Ellis, R. S. 1992, *MNRAS*, 254, 601
- Bruzual, G., & Charlot, S. 2003, *MNRAS*, 344, 1000
- Burstein, D., Faber, S. M., Gaskell, C. M., & Krumm, N. 1984, *ApJ*, 287, 586
- Burstein, D., Davies, R. L., Dressler, A., Faber, S. M., Stone, R. P. S., Lynden-Bell, D., Terlevich, R. J., & Wegner, G. 1987, *ApJS*, 64, 601
- Caldwell, N., Rose, J. A., & Concannon, K. D. 2003, *AJ*, 125, 2891
- Caldwell, N. 1983, *AJ*, 88, 804
- Cappellari, M. *et al.* , 2006, *MNRAS*, 366, 1126
- Cervantes, J. L., & Vazdekis, A. 2009, *MNRAS*, 392, 691
- Chabrier, G. 2003, *PASP*, 115, 763
- Chang, R., Shen, S., Hou, J., Shu, C., & Shao, Z. 2006, *MNRAS*, 372, 199
- Charlot, S., & Bruzual, A. G. 1991, *ApJ*, 367, 126
- Clemens, M. S., Bressan, A., Nikolic, B., & Rampazzo, R. 2008, *MNRAS*, L134
- Cooper, M. C., *et al.* 2008, *MNRAS*, 383, 1058
- Cordier, D., Pietrinferni, A., Cassisi, S., & Salaris, M. 2007, *AJ*, 133, 468
- Cowie, L. L., Songaila, A., Hu, E. M., & Cohen, J. G. 1996, *AJ*, 112, 839
- De Angeli, F., Piotto, G., Cassisi, S., Busso, G., Recio-Blanco, A., Salaris, M., Aparicio, A., & Rosenberg, A. 2005, *AJ*, 130, 116
- Gallazzi, A., Charlot, S., Brinchmann, J., White, S. D. M., & Tremonti, C. A. 2005, *MNRAS*, 362, 41
- Gallazzi, A., Charlot, S., Brinchmann, J., & White, S. D. M. 2006, *MNRAS*, 370, 1106
- Graves, G. J., Faber, S. M., & Schiavon, R. P. 2008, [arXiv:0810.4334](https://arxiv.org/abs/0810.4334)
- Graves, G. J., & Schiavon, R. P. 2008, *ApJS*, 177, 446
- Harris, G. L. H., & Harris, W. E. 2000, *AJ*, 120, 2423

- Hyeop Lee, J., Lee, M. G., Park, C., & Choi, Y.-Y. 2008, arXiv:0807.0110
- Idiart, T. P., Silk, J., & de Freitas Pacheco, J. A. 2007, MNRAS, 381, 1711
- Kaviraj, S., Rey, S.-C., Rich, R. M., Yoon, S.-J., & Yi, S. K. 2007, MNRAS, 381, L74
- Kaviraj, S. 2008, Modern Physics Letters A, 23, 153
- Kelson, D. *et al.*, 2000, ApJ, 529, 768
- Kelson, D. D., Illingworth, G. D., Franx, M., & van Dokkum, P. G. 2001, ApJ, 552, L17
- Kodama, T., & Arimoto, N. 1997, A&A, 320, 41
- Kuntschner, H. 2000, MNRAS, 315, 184
- Larson, R. B. 1974, MNRAS, 166, 585
- Li, Z., & Han, Z. 2007, VizieR Online Data Catalog, 347, 10795
- Lisker, T., & Han, Z. 2008, ApJ, 680, 1042
- MacArthur, L. A., Ellis, R. S., Treu, T., U, V., Bundy, K., & Moran, S. 2008, ApJ, 680, 70
- Matteucci, F. 2006, arXiv:astro-ph/0610832
- Matteucci, F., & Tornambe, A. 1987, A&A, 185, 51
- Mei, S., et al. 2009, ApJ, 690, 42
- Odell, A. P., Schombert, J., & Rakos, K. 2002, AJ, 124, 3061
- Percival, S. M., Salaris, M., Cassisi, S., & Pietrinferni, A. 2009, ApJ, 690, 427
- Rakos, K., & Fiala, N. 1983, PASP, 95, 594
- Rakos, K., & Schombert, J. M. 1995, ApJ, 439, 47
- Rakos, K., & Schombert, J. 2004, AJ, 127, 1502
- Rakos, K., & Schombert, J. 2005, PASP, 117, 245
- Rakos, K., Schombert, J. M., Odell, A. P., & Steindling, S. 2000, ApJ, 540, 715
- Rakos, K. D., Odell, A. P., & Schombert, J. M. 1997, ApJ, 490, 194
- Rakos, K., Schombert, J., & Odell, A. 2007, ApJ, 658, 929
- Rakos, K., Schombert, J., & Odell, A. 2008, ApJ, 677, 1019
- Rose, J. A. 1985, AJ, 90, 1927

- Salaris, M., & Weiss, A. 2002, *A&A*, 388, 492
- Sánchez-Blázquez, P., Gorgas, J., Cardiel, N., & González, J. J. 2006, *A&A*, 457, 809
- Schiavon, R. P. 2007, *ApJS*, 171, 146
- Schombert, J., & Rakos, K. 2009, *AJ*, 137, 528
- Schulz, J., Fritze-v. Alvensleben, U., Möller, C. S., & Fricke, K. J. 2002, *A&A*, 392, 1
- Thomas, D., Maraston, C., Bender, R., & Mendes de Oliveira, C. 2005, *ApJ*, 621, 673
- Trager, S. C., Faber, S. M., Worthey, G., & González, J. J. 2000, *AJ*, 120, 165
- Trager, S. C., Worthey, G., Faber, S. M., & Dressler, A. 2005, *MNRAS*, 362, 2
- Trager, S. C., Faber, S. M., & Dressler, A. 2008, *MNRAS*, 386, 715
- Twarog, B. A. 1980, *ApJ*, 242, 242
- van Dokkum, P. G., & van der Marel, R. P. 2007, *ApJ*, 655, 30
- Visvanathan, N., & Sandage, A. 1977, *ApJ*, 216, 214
- White, S. D. M., & Frenk, C. S. 1991, *ApJ*, 379, 52
- Worthey, G., Faber, S. M., & Gonzalez, J. J. 1992, *ApJ*, 398, 69
- Worthey, G., Trager, S. C., & Faber, S. M. 1995, in Buzzoni, A. & Renzini, A. and Serrano, A., *Astronomical Society of the Pacific Conference Series, Fresh Views of Elliptical Galaxies*, Astronomical Society of the Pacific, 86, 203
- Worthey, G., España, A., MacArthur, L. A., & Courteau, S. 2005, *ApJ*, 631, 820
- Worthey, G. 1994, *ApJS*, 95, 107
- Wyder, T. *et al.* , 2007, *ApJS*, 173, 293
- Wyse, R. F. G., & Gilmore, G. 1995, *AJ*, 110, 2771
- Yi, S. K. 2008, in Heber, U., Jeffery, C. S. & Napiwotzki, R., *Astronomical Society of the Pacific Conference Series*, 392, 3

Table 1. SSP and Multi-Metallicity SED Models

[Fe/H]	$uz - vz$	$vz - yz$	$bz - yz$	$U - B$	$B - V$	$V - K$	$\langle \text{Fe} \rangle$	Mg <sub>b</sub>	H $\beta$
5 Gyr SSP									
-0.7	0.614	0.289	0.202	0.201	0.725	2.387	1.587	2.174	2.053
-0.4	0.646	0.378	0.229	0.280	0.773	2.569	1.937	2.307	2.149
0.0	0.712	0.535	0.276	0.431	0.855	2.867	2.458	2.894	2.080
+0.4	0.794	0.712	0.332	0.595	0.958	3.317	2.900	3.763	1.711
12 Gyr SSP									
-0.7	0.628	0.418	0.238	0.289	0.799	2.522	1.814	2.846	1.561
-0.4	0.690	0.540	0.278	0.415	0.867	2.813	2.191	2.933	1.640
0.0	0.783	0.711	0.329	0.594	0.954	3.116	2.817	3.565	1.610
+0.4	0.909	0.902	0.381	0.797	1.054	3.504	3.219	4.316	1.272
5 Gyr Multi-Metallicity									
-0.7	0.622	0.263	0.200	0.185	0.711	2.363	1.506	1.995	2.174
-0.4	0.643	0.342	0.222	0.251	0.755	2.539	1.811	2.264	2.144
0.0	0.686	0.464	0.260	0.357	0.823	2.851	2.231	2.753	2.046
+0.4	0.737	0.593	0.303	0.467	0.899	3.245	2.610	3.380	1.819
12 Gyr Multi-Metallicity									
-0.7	0.633	0.388	0.238	0.267	0.785	2.515	1.710	2.577	1.702
-0.4	0.671	0.486	0.266	0.360	0.839	2.744	2.059	2.876	1.660
0.0	0.738	0.625	0.308	0.494	0.915	3.066	2.523	3.362	1.574
+0.4	0.811	0.762	0.349	0.624	0.991	3.413	2.890	3.918	1.370